Aqueous-phase Hydrogenation of α-Pinene to *cis*-Pinane Using an Amphiphilic Ni-based Catalyst

Ming-Hao Bao,[a] Feng-Li Yu,[b] Bing Yuan,[b] Cong-Xia Xie,[b,c,*] and Shi-Tao Yu [a,*]

Alpha-pinene is an important forest chemical resource, and the *cis*-pinane obtained by its hydrogenation reaction is used in spices, medicine, and other industries. A hollow nanospheric material with amphiphilic properties in a two-sided structure was prepared, with a nitrogen-doped carbon layer towards the inside and mesoporous silica in the outer layer of the nanospheres. The amphiphilic catalyst with non-precious nickel as the active component was synthesized by loading nickel onto the nanospheres using a simple impregnation method and applied to the aqueous phase hydrogenation reaction of α-pinene. The mesoporous structure of the catalyst shortened the mass transfer distance and thus reduced the mass transfer resistance. The nitrogen atoms doped in the carbon matrix provided anchor points for stabilizing the metal nanoparticles; the hydrophilic outer surface and hydrophobic hollow cavity enabled the catalyst to be well dispersed in water while still enriching the organic matter in aqueous solution. The effect of various reaction conditions on the catalytic reaction was investigated. The catalysts showed excellent activity and good stability, suggesting a new green and efficient method for more effective exploitation of biomass pine resin resources, and providing a reference for expanding the application of non-precious metal catalysts.

DOI: 10.15376/biores.18.2.4032-4054

Keywords: Amphiphilicity; Nickel; α-Pinene; Aqueous phase hydrogenation

Contact information: a: State Key Laboratory Base of Eco-chemical Engineering, College of Chemical Engineering, Qingdao University of Science and Technology, Qingdao, 266042, China; b: College of Chemistry and Molecular Engineering, Qingdao University of Science and Technology, Qingdao, 266042, China; c: Jiangsu Province Biomass Energy and Materials Laboratory, Nanjing, 210042, China;
** Corresponding author: xiecongxia@126.com (X.-C. Xie); yushitaoqust@126.com (S.-T. Yu)*

INTRODUCTION

Turpentine is an important biomass resource that is widely available, inexpensive, and easily accessible. China is a major producer of turpentine, accounting for more than 27% of the world's total production (Nuttens *et al*. 2015), but most of the turpentine resources are directly utilized without further processing, resulting in low utilization. α-Pinene is the main component of turpentine, accounting for 60 to 85% (Desai *et al*. 2017), and due to its special structure, it can undergo a series of chemical reactions, such as hydrogenation, isomerization, and oxidation. The chemical products produced after these chemical reactions are widely used in fragrance, pharmaceutical, textile, paper, and other industries (Berger 2007; Khayyat and Roselin 2018).

Hydrogenation of α-pinene yields *cis*-pinane and *trans*-pinane, which are isomers. Because the C_2-H bond of *trans*-pinane is protected by two methyl groups attached to the same carbon atom on the cyclobutene moiety, the spatial site resistance is increased, and

the secondary hydrogen activity at the C_2 position is reduced compared with that of *cis*-pinane. Hence, the reactivity of *cis*-pinane is much higher than that of *trans*-pinane (Tanielyan *et al*. 2014). The *cis*-pinane obtained by the hydrogenation reaction of α-pinene has high economic value, so it is important to study the deep processing of catalytic hydrogenation of α-pinene from biomass resources (Huang *et al*. 2021).

In heterogeneous catalytic reactions (Duarte *et al*. 2015; Wang *et al.* 2015; Yang *et al.* 2015; Behling *et al*. 2016; Wei *et al.* 2019) and homogeneous catalytic reactions (Hou *et al.* 2015; Shi *et al*. 2017), the catalysts include noble metal catalysts and non-precious metal catalysts, which act as multiphase catalysts (Golets *et al*. 2015). The noble metal catalysts mainly include ruthenium, platinum, palladium, rhodium, and germanium, such as Pd/C, Pt/C, Ru/Al_2O_3, Rh/Al_2O_3, *etc*. (Selka *et al*. 2017; Kalenchuk *et al.* 2018; Liu *et al.* 2018; Moutombi *et al.* 2018; Xiong *et al.* 2020). The non-precious metal catalysts are mainly nickel-based catalysts, such as Raney-nickel (Li *et al*. 2019), Ni-P/Al_2O_3 (Shao *et al*. 2018), spent fluid catalytic cracking catalyst (SFCC) supported nickel (Ni/SFCC) (Wang *et al*. 2015), Ni/$AlPO_4$ (Yang *et al*. 2018), and fluid catalytic cracking catalyst residue (FC3R) supported nickel using layered double hydroxides (LDHs) as the precursor (LP-Ni/FC3R) (Huang *et al*. 2015). The high selectivity and cheap and easy availability of Ni make it stand out among many non-precious metals. Despite their higher activity, precious metals are expensive to produce due to resource scarcity. Non-precious metals are cheaper than precious metals despite their deficiencies in activity, and catalyst carriers also play a key role in stabilizing active sites and enhancing the adsorption of major reactants (Le *et al*. 2016), thus appropriately compensating for the deficiencies of non-precious metals and enhancing their catalytic performance.

For the purpose of ecological protection, there is an increasing focus on the development of green chemistry (Anastas and Williamson 1996). Residual solvents at the end of various chemical reactions cause harm to the environment and human health, and it is important to select solvents that comply with the principles of green chemistry to minimize this harm and to the costs associated with waste disposal and environmental remediation (Zhou *et al*. 2019). Researchers have tried using ethanol and *n*-octane (Deliy and Simakova 2008) as reaction solvents for the catalytic hydrogenation of pinene, and although these organic solvents are widely used in chemical production, they escape into the environment, leading to various atmospheric pollutants (Slater *et al*. 2010). Selka *et al*. (2017) performed the first solvent-free multiphase hydrogenation of pinene on carbon, alumina and silica carriers loaded with metal Pd. The absence of solvent, although environmentally friendly, leads to overheating in practical production.

Water is the only abundant natural solvent on earth; it is cheap, non-toxic, and non-flammable (Borthakur *et al*. 2022). Both water-soluble and insoluble substrates in nature can be transformed in water, and water can be called the greenest solvent. In many cases, water as a solvent not only can accelerate the rate of organic reactions to some extent, but it also can improve the regioselectivity of chemical reactions. Narayan *et al*. (2005) demonstrated that the chemical reaction rate can be enhanced by simply floating water-insoluble organic reactants on top of the solvent water or by dissolving the solids with water as a solvent, a phenomenon known as the "water effect". This demonstrates the feasibility of using water as a solvent for α-pinene catalytic hydrogenation as an environmentally friendly scheme. It also shows the low water solubility of the reaction product, pinane, which can be obtained with a simple phase separation without additional additives.

Herein, to address the current problems of the hydrogenation reaction of α-pinene from biomass resources, a silica-coated mesoporous nanomaterial was prepared with nitrogen doped in carbon, which is characterized by a hollow cavity and amphiphilicity. The hydrophilic silica shell layer on the outside of the material improves the stability of the material and its dispersibility in water, and the nitrogen atoms on the inside of the material create favorable conditions for stabilizing the metal nanoparticles. An amphiphilic nickel-based catalyst was synthesized on top of this mesoporous nanomaterial for the first time, and characterized the catalyst using scanning electron microscopy (SEM), transmission electron microscopy (TEM), contact angle test, X-ray diffraction (XRD), X-ray photoelectron spectroscopy (XPS), high-angle annular dark field scanning transmission electron microscopy (HADDF-STEM), and elemental mapping (STEM-EDX elemental mapping), and investigated the effect of different hydrogen reduction temperatures on the metallization of nickel. Through the screening of the reaction conditions, the catalyst showed good catalytic performance in the aqueous phase hydrogenation reaction of α-pinene, achieving a breakthrough in catalyzing α-pinene hydrogenation reaction in green solvent with a single non-precious metal as the active component, and both the product and the catalyst could be charged by simple phase separation, meeting the requirements of environment-friendly chemistry.

EXPERIMENTAL

Chemicals and Reagents

Cetyltrimethylammonium bromide (CTAB), ethylenediamine (EDA), resorcinol, formaldehyde (37 wt%), tetraethyl silicate (TEOS), nickel acetate tetrahydrate ($NiC_4H_6O_4 \cdot 4H_2O$, 99%), and anhydrous ethanol (99.7%) were purchased from Shanghai Sinopharm Chemical Reagent Co. Nickel chloride hexahydrate ($NiCl_2 \cdot 6H_2O$, 99%) and nickel nitrate hexahydrate ($Ni(NO_3)_2 \cdot 6H_2O$, 99%) were purchased from Shanghai Maclean Biochemical Technology Co. In addition, α-pinene (98%) was purchased from Shanghai Kolaman Reagent Co., Ltd. and high-purity hydrogen (99.99 wt%) and high-purity nitrogen (99.99 wt%) were provided by Qingdao Dehaiye Wei Technology Co. All other used chemicals and reagents were also purchased and used without further purification. Secondary deionized water was used for all experiments.

Preparation of Amphiphilic Hollow Nanomaterials (N-C@MS)

In a typical preparation, 0.12 g of CTAB was dissolved in a mixture of 15 mL ethanol and 35 mL water and stirred for 30 min at room temperature (25 °C). Then, 0.16 mL ethylenediamine was then added and stirring was continued for another 20 min. Subsequently, 0.16 g of resorcinol and 0.24 mL of formaldehyde solution (37 wt%) were added sequentially to the above solution under continuous stirring for 2 h to form polybenzoxazine (PB) balls. Subsequently, 50 mg CTAB and 0.6 mL TEOS were sequentially added, and the solution was stirred for 4 h at room temperature to form PB@MS nanospheres with a core–shell structure. The solid products were collected by centrifugation, washed several times with water and ethanol, and dried at room temperature for two days. The obtained light pink powder was heated to 900 °C at a rate of 5 °C/min under nitrogen atmosphere and calcined at 900 °C for 3 h to obtain the hollow nanomaterial N-C@MS.

Preparation of Amphiphilic Catalysts Loaded with Non-Precious Metal Nickel (Ni/N-C@MS)

N-C@MS (0.1 g) was dispersed in 30 mL ethanol, followed by the addition of a certain amount of $NiC_4H_6O_4{\cdot}4H_2O$ and sonication for 20 min to ensure good dispersion. The resulting mixture was magnetically stirred at room temperature for 4 h. The ethanol solvent was removed via spin evaporation at 55 °C using a rotary evaporator. After natural drying at room temperature, the solid material was transferred to a tube furnace under hydrogen atmosphere and maintained at 550 °C for 4 h, yielding the amphiphilic nanocatalyst Ni/N-C@MS.

α-Pinene Hydrogenation Reaction

In a typical reaction, α-pinene (1.0 g) and 0.05 g of the synthesized catalyst were added to a 50 mL PTFE-lined autoclave. Subsequently, hydrogen was charged into the autoclave, and the air in the kettle was discharged by displacing it with 1 MPa hydrogen three times. Then, 3 MPa hydrogen was charged. The autoclave was put in an oil bath at 120 °C, and the mixture was stirred magnetically for 3 h with the temperature inside the kettle measured with a thermometer.

After the reaction, the solution was removed, and after the addition of 1 mL *n*-heptane, the solution was centrifuged and left to stand for 10 min. The supernatant was analyzed by gas chromatography with an OV-1701 capillary column (30 mm × 0.25 mm × 0.33 μm). For the recycling of the catalyst, the catalyst can be separated from the solvent water by centrifugation at the end of each reaction and used again after vacuum drying at 60 °C.

Catalyst Characterization

Scanning electron microscope (SEM) images were taken on a JEOL JSM-7610F field emission scanning electron microscope. Transmission electron microscope (TEM) images were obtained on a JEOL JEM-2100 field emission transmission electron microscope. High-angle annular dark-field scanning TEM (HAADF-STEM) and energy dispersive X-ray (EDX) elemental mapping images were taken on a TALOS F200X G2 high-resolution transmission electron microscope.

Elemental analysis of catalysts was performed using a PerkinElmer ICP 2100 inductively coupled plasma emission spectrometer.

N_2 adsorption-desorption isotherms were obtained on a Micromeritics ASAP 2020 adsorber. Brunner-Emmett-Teller (BET) surface area was calculated from the linear part of the BET plot. The pore size distribution was calculated from the adsorption branch of the isotherm by the BJH method.

Water droplet contact angles were tested by a JCY-4 contact angle meter. X-ray photoelectron spectroscopy (XPS) spectra were obtained using a Thermo ESCALAB 250XI spectrometer. The Raman spectrograms of the materials were measured on a LabRAM HR-800 laser confocal Raman spectrometer.

The thermo-gravimetric curves of the carriers were measured on a DZ-TGA105 thermogravimetric analyzer. XRD images of the materials were obtained by using an X-ray diffractometer XRD-7000.

RESULTS AND DISCUSSION

Preparation and Characterization of Ni-loaded Amphiphilic Nanocatalysts

The catalyst carriers with amphiphilic properties were prepared as shown in Fig. 1. PB spheres were synthesized using a typical sol–gel polymerization method. The PB spheres were then uniformly coated with a silica shell on the outside using TEOS as the silica precursor and CTAB as the templating agent. Because of the protective effect of the outer silica shell, the PB spheres can undergo domain-limited carbonization at 900 °C under nitrogen atmosphere and decompose from the inside to the outside, transforming into nitrogen-doped hollow carbon shells (N-C) and a part of the carbon shells are embedded in the mesoporous SiO_2 shell layer, forming hollow mesoporous nanospheres with a two-sided structure. The formation of hollow cavities inside the nanospheres was due to the decomposition of PB spheres at high temperature. It is noteworthy that PB spheres have weak cross-linking properties. Therefore, they are decomposed by heat in an inside-out direction. A hollow cavity structure is eventually formed owing to the domain-limiting guidance of the external SiO_2 shell. The preparation of mesoporous nanomaterials using this domain-limited pyrolysis method has been reported previously, but the polymers used often decomposed from the outside to the inside (Xu *et al.* 2008; Davis *et al.* 2012), leading to incomplete decomposition and formation of yolk–shell structure rather than a hollow cavity. Amphiphilic catalysts loaded with Ni were obtained by loading the active component (metal Ni) onto the carrier using the impregnation–hydrogen reduction method.

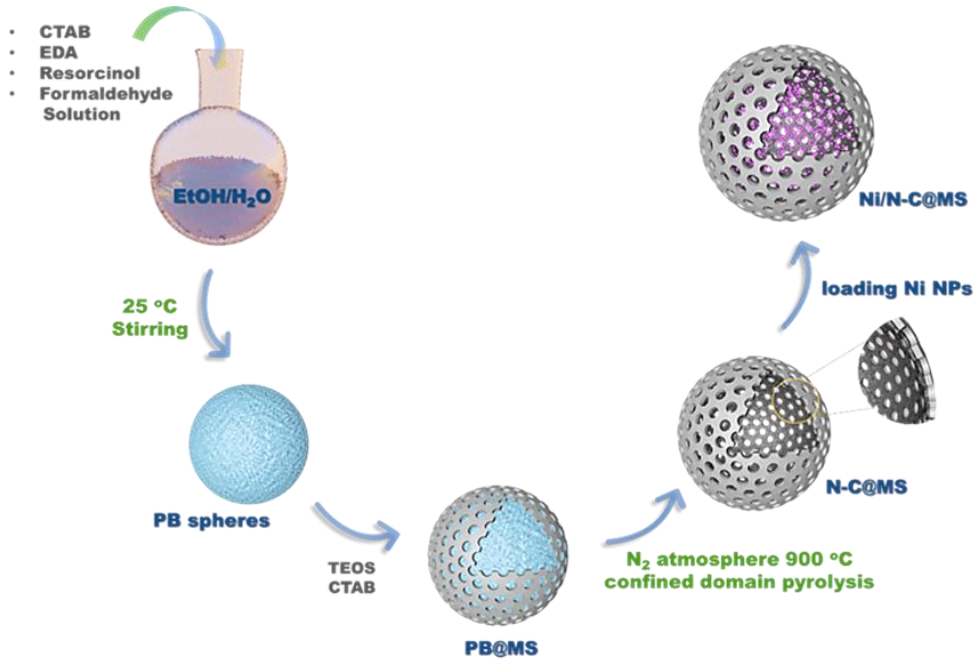

Fig. 1. Preparation of amphiphilic catalysts Ni/N-C@MS

First, the morphology of N-C@MS was characterized (Fig. 2). SEM images (Fig. 2a, b) show that the material has a uniform spherical morphology with an average particle size of approximately 340 nm. TEM images (Fig. 2c, d) show that each N-C@MS nanosphere contains a large cavity and has a shell layer thickness of approximately 50 nm. The HAADF-STEM images (Fig. 2e) further demonstrate the hollow spherical structure of

the material. The STEM-EDX elemental mapping images (Fig. 2f-i) show the distribution of each constituent element in the material, including C, N, O and Si. As shown in Fig. 2f and g, C and N were mainly present on the inner surface of the nanospheres, where the presence of N was very helpful for anchoring the metal nanoparticles with catalytic activity.

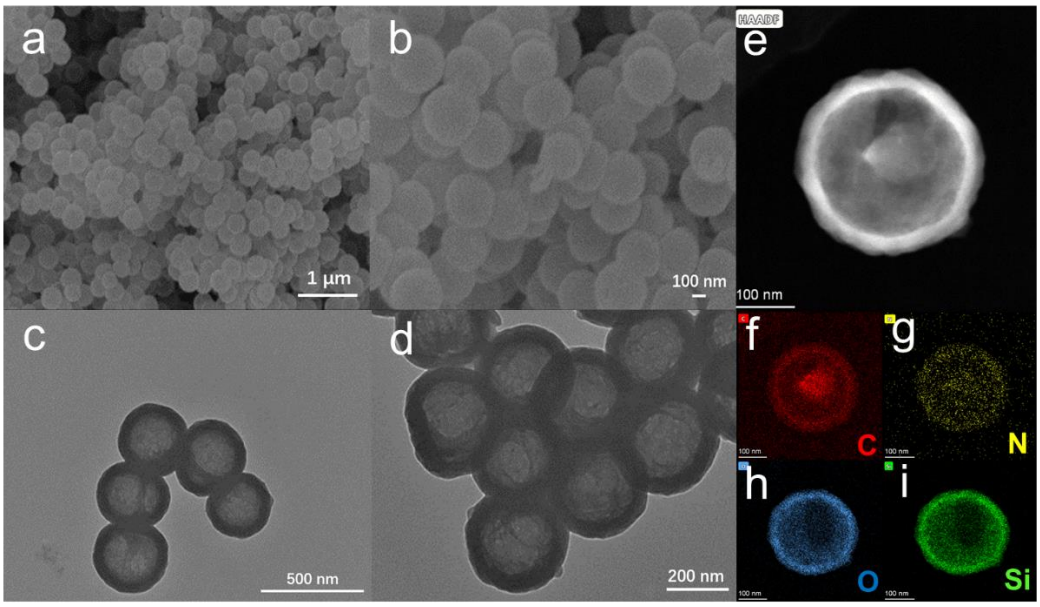

Fig. 2. SEM images (a, b), TEM images (c, d), HAADF-STEM image (e), and STEM-EDX elemental mapping images (f–i) of N-C@MS

The structure of the nanospheres was characterized using N_2 adsorption–desorption isotherms (Fig. 3a). The images show a clear upward trend in the N_2 adsorption–desorption isotherm at the relative pressure P/P_0 in a lower range (0 to 0.05) and higher range (0.2 to 1.0), which indicates the presence of both microporous and mesoporous structures in the nanospheres.

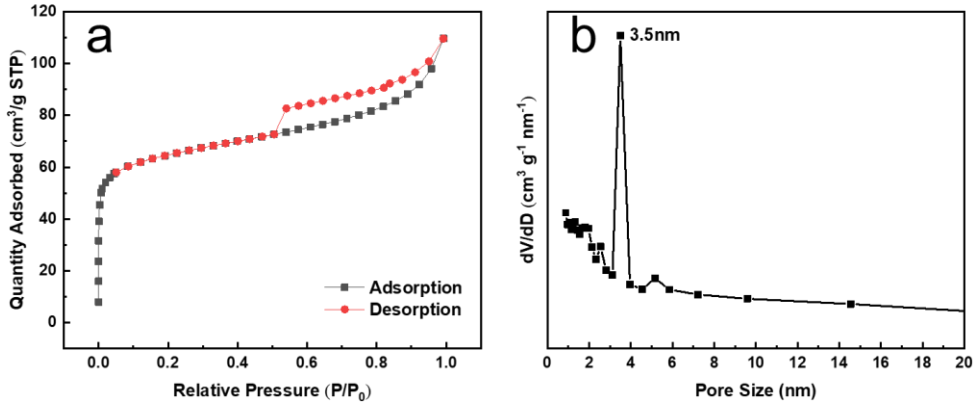

Fig. 3. N_2 adsorption/desorption isotherms (a) and BJH pore diameter distribution curves of N-C@MS (b)

An H3-type hysteresis loop can also be observed in the curve for the relative pressure P/P_0 in the range of 0.5 to 1.0, indicating the presence of cavities inside the

nanospheres. The calculated Brunauer–Emmett–Teller specific surface area of the material was 200 m^2/g, and the corresponding Barrett–Joyner–Halenda (BJH) pore size distribution curve is shown in Fig. 3b. The nanomaterials had uniform mesopores with a pore size of 3.5 nm and a pore volume of approximately 0.16 cm^2/g. The uniform mesopore structure and large cavities inside the nanospheres are not only beneficial to the loading of the active component (metal nanoparticles), but they can also shorten the diffusion path of the reactants in the carrier during the catalytic reaction, thus enhancing the catalytic performance.

The material had an N-C layer on the inside and a silica shell layer on the outside. This two-sided structure endowed the nanospheres with superior amphiphilic properties (hydrophilic and hydrophobic). The amphiphilic properties of N-C@MS were characterized using a water droplet contact angle test (Fig. 4). The water droplet contact angle of the N-C layer inside the nanospheres was 86.1° (Fig. 4a). It should be noted that the contact angle inside the nanospheres was determined using the N-C material without the outer silica shell. After the PB spheres was prepared, as shown in Fig. 1, the next step of adding TEOS and CTAB was not performed. The PB spheres was directly calcined with argon gas to provide N-C material. The final calcined material was subjected to water droplet contact angle test, to obtain the water droplet contact angle inside the N-C@MS nanospheres. The water droplet contact angle of the external mesoporous silica shell was 19.5° (Fig. 4b), and that of N-C@MS was 26.6° (Fig. 4c). This demonstrates that the nanospheres had a two-sided structure. They were hydrophobic in the interior and had a hydrophilic shell.

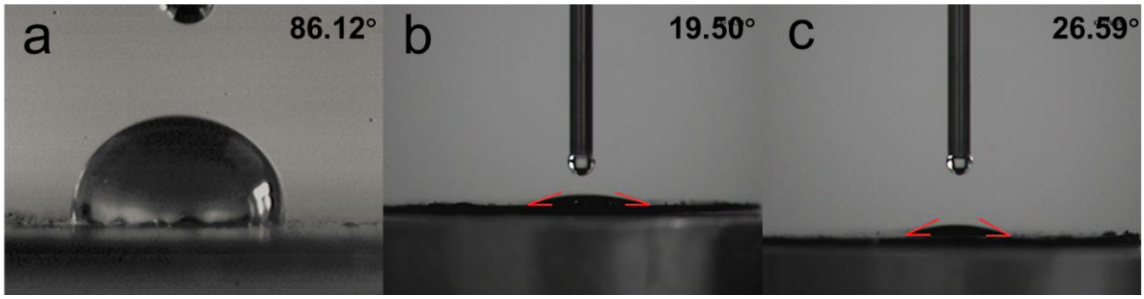

Fig. 4. Water-drop contact angles of N-C (a), MS (b), and N-C@MS (c)

The full-sweep XPS spectrum (Fig. 5a) exhibits representative peaks of N-C@MS for C1s, N1s, O1s, and Si2p. The contents of elemental C and N in N-C@MS using C/H/N elemental analysis were 31.3% and 1.68%, respectively. The high-resolution XPS spectra of C1s (Fig. 5b) showed three characteristic peaks of functional groups, namely the C=C characteristic peak with binding energy at 284.5 eV, the C-N characteristic peak with binding energy at 285.5 eV, and the O-C=O characteristic peak with binding energy at 287.1 eV (Zhou *et al.* 2015).The high-resolution XPS N1s spectrum (Fig. 5c) shows three characteristic peaks of nitrogen, indicating that the material was composed of three types of structural nitrogen atoms with binding energies of 401.3 eV, 399.5 eV, and 397.8 eV. These peaks correspond to graphitic, pyrrolic, and pyridinic nitrogen, respectively (Wang *et al.* 2018). The contents of pyridinic and pyrrolic nitrogen contents were much higher than the graphitic nitrogen content, and the high pyridinic nitrogen content is helpful for immobilizing metal nanoparticles (Yin *et al.* 2019). In the O1s high-resolution XPS spectrum (Fig. 5d), the peaks located at 534.1 eV, 533.5 eV, and 532.9 eV correspond to COOH, C–O and C=O groups, respectively (Hulicova-Jurcakova *et al.* 2008).

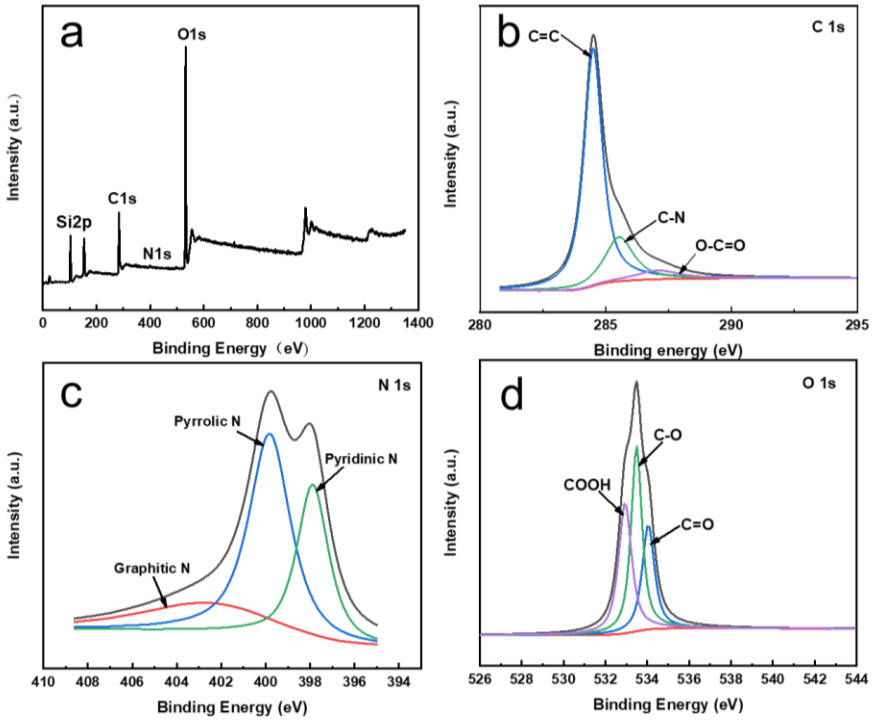

Fig. 5. XPS full sweep spectra of materials N-C@MS (a), high resolution XPS spectra of C1s (b), high resolution XPS spectra of N1s (c), high resolution XPS spectra of O1s (d)

The Raman spectrum of the material (Fig. S1, see Appendix) shows two distinct peaks at 1329 and 1588 cm^{-1}, corresponding to the typical D and G energy bands of the carbon-containing material. The D energy band is a characteristic peak indicating the presence of disordered carbon, indicating material doping and defects. The G energy band is a characteristic peak of graphitized carbon. The ratio of the intensities of the two peaks is an important indicator of the degree of graphitization of the material. The ID/IG value indicates the degree of defects in N-C@MS, which may be caused by the thermal decomposition of PB during the domain-limited carbonization. The thermogravimetric curve (Fig. S2) of N-C@MS shows a significant decrease in weight after 600 °C, which indicates that the material had good thermal stability.

The active component non-precious metal Ni nanoparticles were loaded onto the N-C@MS nanosphere carrier by a simple impregnation-hydrogen reduction method. The TEM image (Fig. 6a, b) shows that the metallic Ni nanoparticles were successfully loaded onto the carrier and uniformly dispersed in the N-C@MS hollow mesoporous nanospheres, with the presence of Ni nanoparticles in both the outer shell and the cavity of the nanospheres. The loading of metal Ni by ICP elemental test was 12.5 wt%. The high-resolution TEM image (Fig. 6c) shows that the Ni nanoparticles in the Ni/N-C@MS catalyst had distinct lattice stripes. The face spacing of the lattice stripes was measured to be 0.2 nm, which was attributed to the Ni (111) crystal plane (Xie *et al.* 2021). The histogram of particle size (Fig. 6d) shows that the size of Ni nanoparticles in the catalyst was within the range of 2.6 to 5.6 nm, with an average particle size of 4.1 nm. The homogeneous size of the metal nanoparticles is attributed to the coordination anchoring effect of the N atoms doped in the carbon skeleton. In the HAADF-STEM image of Ni/N-C@MS (Fig. 6e), the bright spots distributed on the hollow nanospheres indicate the

locations of the loaded Ni nanoparticles, further confirming the successful loading of metallic Ni. At the same time, the loading of Ni did not have any effect on the morphology and structure of the carrier. Elemental maps of the catalyst (Fig. 6f-j) show the distributions of C, N, O, Si and Ni. The combination of HAADF-STEM images shows that Ni was dispersed inside the cavities of the nanospheres and on the external SiO_2 surface. The EDX full-sweep spectra (Fig. S3) also confirm the presence of elemental Ni in the catalyst.

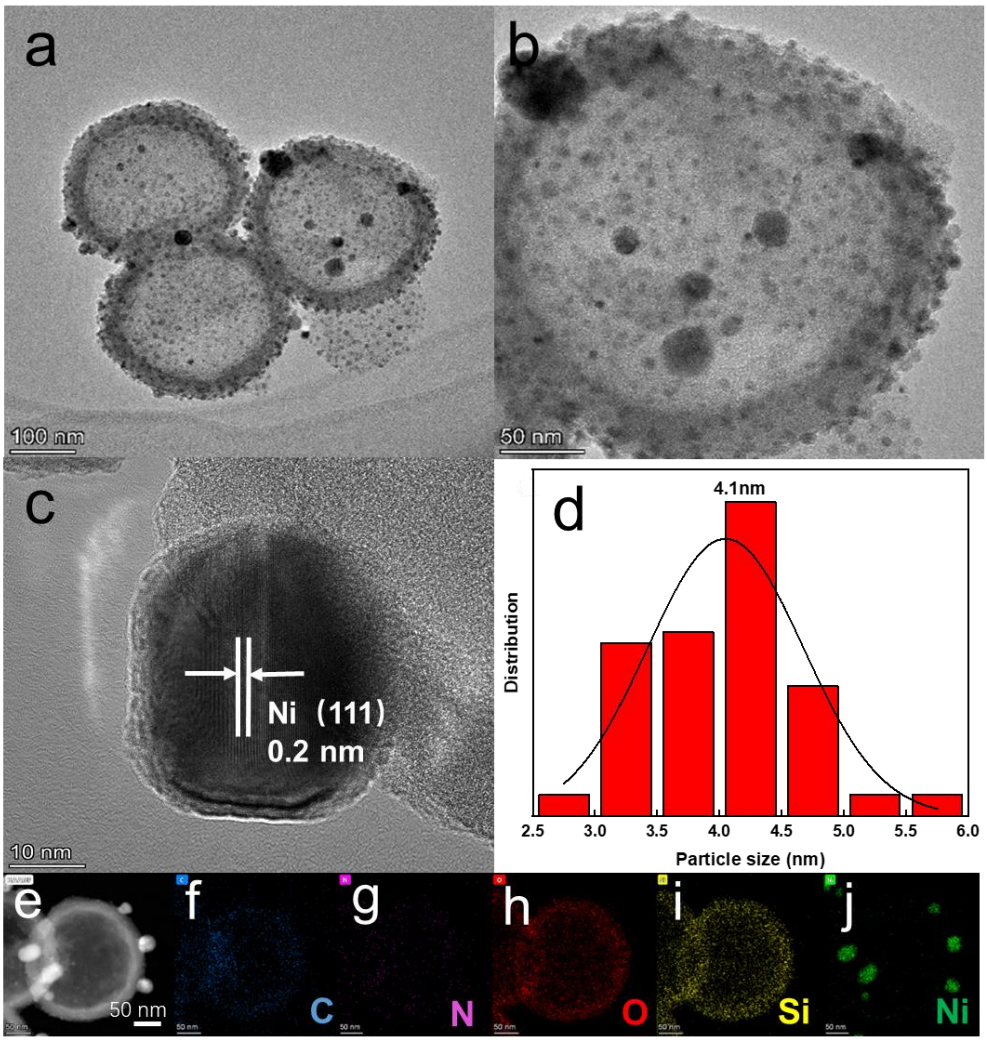

Fig. 6. TEM images (a, b), high-resolution TEM image (c), particle size of distribution of Ni nanoparticles (d), and STEM-EDX elemental mapping images of Ni/N-C@MS (e-j)

The crystal structure of the catalysts was analyzed by XRD. As shown in Fig. 7, the wide-angle XRD spectrum of Ni/N-C@MS exhibits a broad C (002) diffraction peak at 23°, which can be considered the characteristic peak of carbon in the catalyst. The diffraction peaks at positions 44°, 52°, and 76° correspond to the (111), (200), and (220) crystal planes of pure Ni with a face-centered cubic structure, respectively (Li *et al.* 2010). Thus, the XRD results indicate that no crystals other than carbon or pure Ni were present in the catalyst.

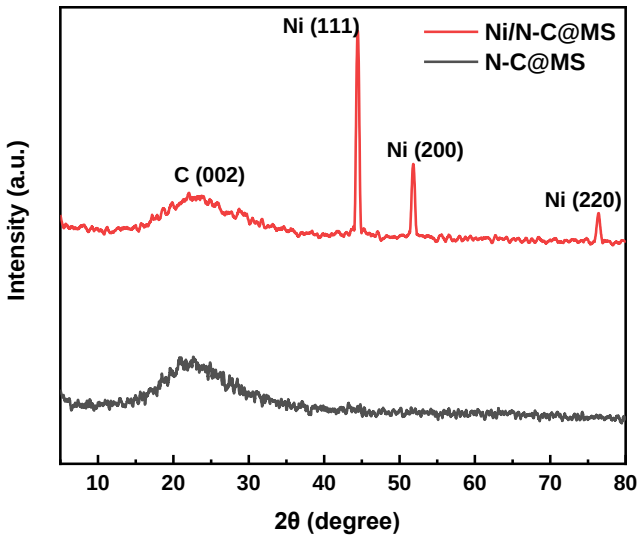

Fig. 7. XRD images of catalyst before and after metal loading

The chemical composition of Ni/N-C@MS was further investigated by XPS. The XPS full-sweep spectrum of Ni/N-C@MS (Fig. 8a) shows that the catalyst consisted of C, N, O, Si, and Ni. A weaker Ni2p peak than in the XPS full-sweep spectrum of the carrier indicated that the active component (Ni nanoparticles) was successfully introduced into the nanosphere carrier. The high-resolution Ni2p XPS spectrum is shown in Fig. 8b, where the peaks centered at the bond energies of 854.6 eV and 872.5 eV correspond to Ni^0, and the percentage of metallic Ni is 31.28%. The peaks centered at the bond energies of 857.5 eV and 875.3 eV are peaks of Ni^{2+}, and the percentage of the peaks is 40.22%. The peaks centered at the bond energies of 862.8 eV and 881.3 eV are the satellite peaks of Ni2p. Different Ni states can affect the surface properties of the catalysts, thus their activity (Wang *et al.* 2021).

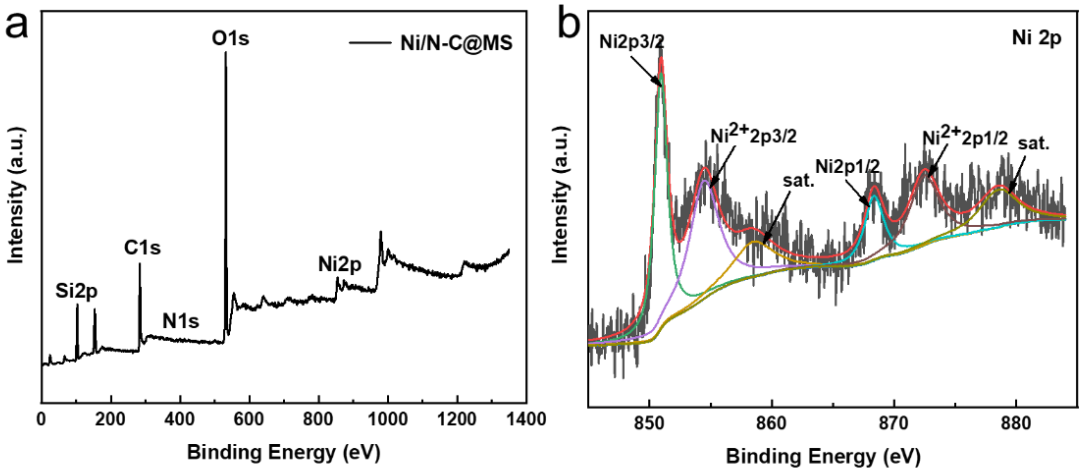

Fig. 8. XPS full sweep spectra of catalyst Ni/N-C@MS (a) and high resolution XPS spectra of Ni2p (b)

The effect of different hydrogen reduction temperatures on the reduction of active component Ni nanoparticles was investigated. The reduction was conducted at the hydrogen concentration of 85% (v/v), heating rate of 2 °C/min, and reduction time of 4 h. The tested reduction temperatures were 450, 500, 550, and 650 °C. The degree of Ni metallization is shown in Fig. 9a. At a reduction temperature of 450 °C, the degree of Ni metallization was 23.9%, which is low. However, with the increase in the reduction temperature, the degree of Ni metallization also gradually increased. At a reduction temperature of 550 °C, the degree of Ni metallization was 35.7%. At the same time, further increase in the reduction temperature to 650 °C resulted in a decrease in the metallization of Ni. The corresponding XRD spectra (Fig. 9b) show that with increasing reduction temperature, the diffraction peaks of the three crystalline planes of Ni first increased and then decreased. The XPS full-sweep spectra at different reduction temperatures (Fig. 9c) and the XPS high-resolution spectra of Ni2p (Fig. 9d) also show consistent results. Integration of the peaks of different valence states of Ni in the XPS high-resolution spectra of Ni2p demonstrates that the proportion of monomeric Ni gradually increased with the increase in reduction temperature from 450 to 550 °C. However, the increase in reduction temperature from 550 to 650 °C resulted in a decrease in the proportion of monomeric Ni. This phenomenon was attributed to the fact that at the reduction temperature lower than 550 °C, more and more Ni was reduced as the temperature increased. However, when the reduction was conducted at higher temperatures, exceedingly high temperatures may have caused Ni agglomeration, resulting in Ni not being fully reduced.

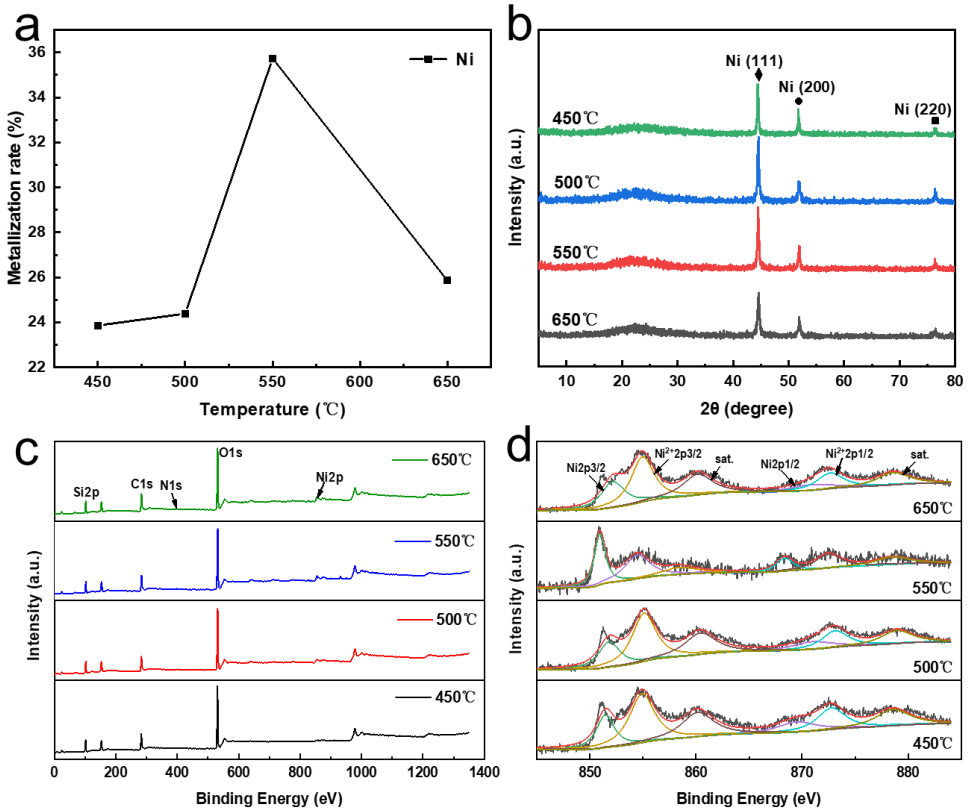

Fig. 9. Effect of reduction temperature on the Ni metallization rate (a), XRD spectra (b), XPS full-sweep spectra (c), and high-resolution Ni2p XPS spectra of Ni/N-C@MS obtained at different hydrogen reduction temperatures (d)

Ni/N-C@MS Catalyzed Reaction

The prepared catalysts were applied to the aqueous-phase hydrogenation of α-pinene from biomass resources for the preparation of *cis*-pinane. Figure 10 shows the schematic diagram of the reaction. The above catalysts were first used at different temperatures to catalyze the α-pinene hydrogenation reaction under aqueous phase conditions to compare their catalytic performance, setting the initial reaction conditions as 120 °C, H_2 pressure 3 MPa, solvent water volume 4 mL, reaction time 3 h and stirring speed 450 rpm. The reaction results are shown in Table 1. The results showed that the catalysts with reduction at 550 °C possessed better catalytic effect, which was consistent with the characterization results.

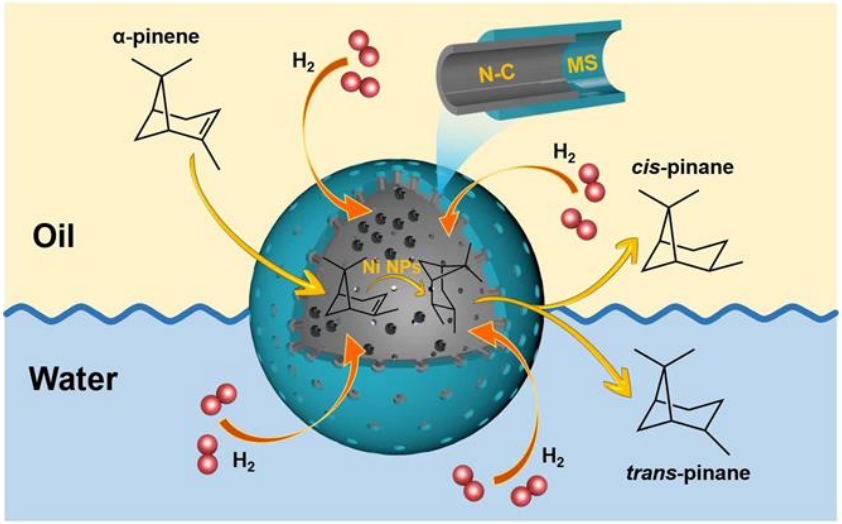

Fig. 10. Principle diagram of the aqueous phase hydrogenation reaction of α-pinene catalyzed by Ni/N-C@MS

Table 1. Comparison of Catalytic Effect of Catalysts with Different Reduction Temperatures

Reduction Temperature (°C)	Conversion of α-Pinene (%)	Selectivity of *cis*-Pinane (%)
450	95.9	93.6
500	93.8	95.3
550	99.7	95.1
650	90.4	94.3
120 °C, 3MPa, 4 mL H_2O, 0.05 g catalyst, 450 rpm, 3 h		

The effect of using different Ni precursors on the hydrogenation reaction of α-pinene during the impregnation loading process was investigated by keeping the other synthesis conditions of the catalyst unchanged at a reduction temperature of 550 °C. Anhydrous ethanol was used as the solvent for the impregnation process, and the reaction results are shown in Table 2. The conversion of α-pinene and the selectivity of *cis*-pinane were the highest when $NiC_4H_6O_4{\cdot}4H_2O$ was used as the Ni precursor. The reason for this is that the organonickel salt has a unique anionic element type and spatial size, and the solubility of the impregnation solution can be significantly increased by the dissolution of organonickel, thus greatly improving the active component content of the catalyst.

Table 2. Effect of Using Different Nickel Sources on the Hydrogenation Reaction of α-Pinene when Loaded with Metals

Precursor	Solvent during Loading	Conversion of α-Pinene (%)	Selectivity of *cis*-Pinane (%)
$NiC_4H_6O_4 \cdot 4H_2O$	ethanol	99.7	95.1
$Ni(NO_3)_2 \cdot 6H_2O$	ethanol	92.9	93.6
$NiCl_2 \cdot 6H_2O$	ethanol	54.3	94.2
120 °C, 3MPa, 4 mL H_2O, 0.05 g catalyst, 450 rpm, 3 h			

The catalysts synthesized under optimal conditions were used to optimize the process conditions for participation in the aqueous phase hydrogenation reaction of α-pinene. As shown in Fig. S4, the conversion of α-pinene was low at temperatures below 100 °C, but it significantly increased with the reaction temperature. At temperatures above 100 °C, the conversion of α-pinene was high, reaching almost complete conversion at 120 °C. The selectivity of *cis*-pinane did not change significantly with increasing temperature and was always approximately 95%. As shown in Fig. S5, at the H_2 pressure below 3 MPa, the catalytic conversion of α-pinene and the selectivity for *cis*-pinane were both relatively low. Both first gradually increased with pressure and then stabilized. The addition of water improved the dispersion of the amphiphilic catalyst. The reaction system without water added resulted in a very low conversion of α-pinene and selectivity for *cis*-pinane. Apparently, both values continuously increased with increasing water volume. However, the conversion of α-pinene and the selectivity of *cis*-pinane decreased when the amount of solvent water was increased to 7 mL, which was due to the fact that the excess solvent water broke the equilibrium relationship of the gas-liquid-solid triple phase, as shown in Fig. 10, thus leading to the decrease of the reaction efficiency (Fig. S6). In addition, the catalyst dosage (Fig. S7) and stirring speed (Fig. S8) were screened. The conversion of α-pinene significantly increased with the extension of the reaction time (Fig. S9). The reaction proceeded almost to completion in 3 h. Combining the results of the above exploration of the reaction conditions, the optimal conditions for the hydrogenation of 1.0 g α-pinene were with a water amount of 4 mL, catalyst addition of 50 mg, reaction temperature of 120 °C, H_2 pressure of 3.0 MPa, and reaction time of 3 h. The catalytic conversion of α-pinene was 99.7% and the selectivity of *cis*-pinane was 95.1% under the optimal conditions, indicating that the amphiphilic catalyst Ni/N-C@MS has excellent catalytic performance and high selectivity.

For comparison, noble metal nanoparticles (Ru, Pd, Pt, Rh) and non-precious metal nanoparticles (Co, Mo, Cr) were loaded onto the amphiphilic material N-C@MS for the aqueous-phase catalytic hydrogenation of α-pinene under the same reaction conditions. In addition, the catalytic performances of some industrially commonly used hydrogenation catalysts were investigated, and the results are listed in Table 3. According to the results in the table, the catalytic performance of Ni/N-C@MS catalysts was significantly better than that of other non-precious metal catalysts under the same reaction conditions, and Ni/N-C@MS catalysts obtained catalytic activities almost equal to those of loaded precious metal catalysts and industrial precious metal catalysts under this reaction condition. The excellent catalytic performance can be attributed on the one hand to the amphiphilic and hollow porous structure of the catalyst carrier. This property not only improves the catalyst dispersion in water, but also reduces the mass transfer resistance by confining the solvent water in the hydrophobic nanopores, allowing it to be used as a tunable solvent. The applied pressure forces a heterogeneous mixture of insoluble molecules and water into the

hydrophobic nanopores inside the material, a behavior that reduces the polarity of water and enhances solubility, thus greatly increasing the effectiveness of the reaction (Ryzhikov *et al.* 2015; Kirschhock *et al.* 2016; Breynaert *et al.* 2020). On the other hand, the excellent catalytic performance also can be attributed to the good selectivity and activity of the active component Ni nanoparticles anchored by N atoms inside the carrier.

Table 3. Hydrogenation of α-Pinene Catalyzed by Different Catalysts

Entry	Catalyst	Conversion of α-pinene (%)	Selectivity of *cis*-pinane (%)
1	Ni/N-C@MS	99.7	95.1
2	Ru/N-C@MS	99.9	99.9
3	Pd/N-C@MS	99.9	89.7
4	Pt/N-C@MS	99.2	98.6
5	Rh/N-C@MS	99.9	94.9
6	Co/N-C@MS	59.7	86.4
7	Mo/N-C@MS	53.2	87.2
8	Cr/N-C@MS	76.6	81.8
9	Raney-Ni	58.1	97.3
10	Ru/C	99.9	98.8
11	Pd/C	99.6	88.0
120 °C, 3MPa, 4 mL H_2O, 0.05 g catalyst, 450 rpm, 3 h			

The catalyst was separated from the reaction mixture by centrifugation at the end of the reaction and used for the next reaction cycle after vacuum drying. Examination of the performance of the catalyst for cycling in the α-pinene hydrogenation reaction (Fig. 11) indicates that Ni/N-C@MS had good stability and could be repeatedly used six times without significant activity loss (conversion of α-pinene and the selectivity for *cis*-pinane above 95%). After the seventh cycle, the conversion of α-pinene decreased to 93%, and the conversion of α-pinene and the selectivity of *cis*-pinane both decreased after the 8th cycle. This result may be attributed to the oxidation and shedding of active Ni nanoparticles. The catalyst was characterized by ICP testing after 8 cycles, and the results showed that the content of active component nickel in the catalyst from 12.5 wt% decreased to 4.1 wt%, indicating a large loss of Ni during the cycling process.

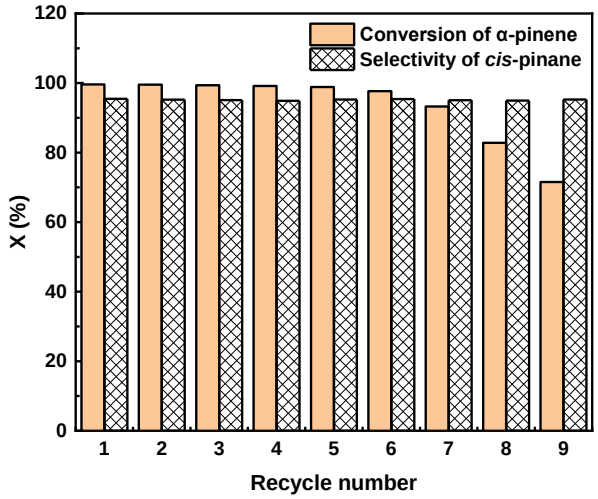

Fig. 11. Recycle performance of Ni/N-C@MS (120 °C, 3 MPa, 3 h)

CONCLUSIONS

1. The amphiphilic hollow nanomaterial N-C@MS was prepared by sol-gel polymerization and high-temperature domain-limited carbonization. Nitrogen atoms doped in the carbon matrix were able to provide anchor sites for stabilizing metal nanoparticles, and the hydrophilic outer surface and hydrophobic hollow cavities enabled the material to be well dispersed in water while still enriching organic matter in aqueous solution with good adsorption and catalytic properties.
2. A catalyst with amphiphilic nature, Ni/N-C@MS, was synthesized by loading non-precious metal nickel nanoparticles onto N-C@MS using a simple impregnation reduction method. The catalyst was used to catalyze the hydrogenation reaction of α-pinene with water as the solvent, and Ni/N-C@MS was found to have good catalytic activity and stability. The conversion of α-pinene reached 99.7%, the selectivity of the target product *cis*-pinane reached 95.1%, and the catalyst could be reused more than 7 times under the reaction conditions of 120 °C, 3 MPa H_2 pressure, 4 mL water, 450 rpm and 3 h. The activity was significantly higher than that of non-precious metal catalysts with Co, Mo, *etc*. as active components, and comparable to that of catalysts containing precious metals such as Ru, Pt, and Pd. The amphiphilic nature of the catalyst makes it suitable for catalyzing reactions in which water is the solvent, which meets the requirements of environment-friendly catalysis and has obvious advantages in both economic and environmental aspects and has a broad application prospect.
3. The α-pinene hydrogenation is an important production process in the forestry chemical industry. This study provides a guideline for the effective utilization of natural biomass resources α-pinene and the green and efficient preparation of pinane products with high *cis*/*trans* isomerization ratio.

ACKNOWLEDGMENTS

The authors are grateful for financial support from the National Natural Science Foundation of China (32071710), the Shandong Provincial Natural Science Foundation of China (ZR2020MC155), and the Open Project of Jiangsu Province Biomass Energy and Materials Laboratory (JSBEM201901).

REFERENCES CITED

Anastas, P. T., and Williamson, T. C. (1996). "Green chemistry: An overview," *J. Green Chemistry* 626(1), 1-17. DOI: 10.1021/bk-1996-0626.ch001

Behling, R., Valange, S., and Chatel, G. (2016). "Heterogeneous catalytic oxidation for lignin valorization into valuable chemicals: What results? What limitations? What trends?," *J. Green Chemistry* 18(7), 1839-1854. DOI: 10.1039/c5gc03061g

Berger, R. G. (2007). *Flavours and Fragrances: Chemistry, Bioprocessing and Sustainability*, G. Bruce (ed.), Springer Science & Business Media, New York, NY. DOI: 10.1007/b136889

Borthakur, I., Kumari, S., and Kundu, S. (2022). "Water as a solvent: Transition metal catalyzed dehydrogenation of alcohols going green," *J. Dalton Transactions* 51(32),

11987-12020. DOI: 10.1039/d2dt01060g

Breynaert, E., Houlleberghs, M., Radhakrishnan, S., Grübel, G., Taulelle, F., and Martens, J. A. (2020). "Water as a tuneable solvent: A perspective," *J. Chemical Society Reviews* 49(9), 2557-2569. DOI: 10.1039/c9cs00545e

Davis, S. E., Ide, M. S., and Davis, R. J. (2012). "Selective oxidation of alcohols and aldehydes over supported metal nanoparticles," *J. Green Chemistry* 15(1), 17-45. DOI: 10.1039/c2gc36441g

Deliy, I. V., and Simakova, I. L. (2008). "Kinetics and thermodynamics of liquid phase isomerization of α-and β-pinene over Pd/C catalyst," *J. Reaction Kinetics and Catalysis Letters* 95(1), 161-174. DOI: 10.1007/s11144-008-5406-3

Desai, N. C., Chudasama, J. A., Patel, B. Y., Jadeja, K. A., Karkar, T. J., Mehta, J. P., and Godhani, D. R. (2017). "Catalysis by the entangled complexes in matrix structure of zeolite-Y over α-pinene," *J. Microporous and Mesoporous Materials* 242, 245-255. DOI: 10.1016/j.micromeso.2017.01.023

Duarte, T. A., Estrada, A. C., Simões, M. M., Santos, I. C., Cavaleiro, A. M., Neves, M. G. P., and Cavaleiro, J. A. (2015). "Homogeneous catalytic oxidation of styrene and styrene derivatives with hydrogen peroxide in the presence of transition metal-substituted polyoxotungstates," *J. Catalysis Science & Technology* 5(1), 351-363. DOI: 10.1039/c4cy00702f

Golets, M., Ajaikumar, S., and Mikkola, J. P. (2015). "Catalytic upgrading of extractives to chemicals: Monoterpenes to "EXICALS"," *J. Chemical Reviews* 115(9), 3141-3169. DOI: 10.1021/cr500407m

Hou, S. L., Xie, C. X., Zhong, H., and Yu, S. T. (2015). "Mild water-promoted ruthenium nanoparticles as an efficient catalyst for the preparation of cis-rich pinane," *J. RSC Advances* 5(109), 89552-89558. DOI: 10.1039/c5ra15283f

Huang, P. P., Deng, Q., Jiang, L. H., Zhi, Y. F., Yang, W. J., Huang, J. Y., Zheng, Y. E., Wang, Y. M., Shan, S. Y., Hu, T. D., and Su, H. Y. (2021). "The exploration of sensitive factors for the selective hydrogenation of α-pinene over recyclable Ni-B/KIT-6 catalyst," *J. Catalysis Letters* 152(8), 2352-2365. DOI: 10.1007/s10562-021-03811-5

Huang, Y. Y., Chen, X. P., Deng, Y. F., Zhou, D., and Wang, L. L. (2015). "A novel nickel catalyst derived from layered double hydroxides (LDHs) supported on fluid catalytic cracking catalyst residue (FC3R) for rosin hydrogenation," *J. Chemical Engineering Journal* 269, 434-443. DOI: 10.1016/j.cej.2015.01.098

Hulicova-Jurcakova, D., Seredych, M., Lu, G. Q., and Bandosz, T. J. (2008). "Combined effect of nitrogen-and oxygen-containing functional groups of microporous activated carbon on its electrochemical performance in supercapacitors," *J. Advanced Functional Materials* 19(3), 438-447. DOI: 10.1002/adfm.200801236

Kalenchuk, A. N., Koklin, A. E., Bogdan, V. I., and Kustov, L. M. (2018). "Hydrogenation of naphthalene and anthracene on Pt/C catalysts," *J. Russian Chemical Bulletin* 67(8), 1406-1411. DOI: 10.1007/s11172-018-2232-2

Khayyat, S. A., and Roselin, L. S. (2018). "Recent progress in photochemical reaction on main components of some essential oils," *J. Journal of Saudi Chemical Society* 22(7), 855-875. DOI: 10.1016/j.jscs.2018.01.008

Kirschhock, C. E., De Prins, M., Verheijen, E., Ryzhikov, A., Daou, T. J., Nouali, H., Taulelle, F., Martens, J. A., and Patarin, J. (2016). "Intrusion–extrusion spring performance of–COK-14 zeolite enhanced by structural changes," *J. Physical Chemistry Chemical Physics* 18(28), 18795-18801. DOI: 10.1039/c6cp03162e

Le, T. A., Kim, M. S., Lee, S. H, Kim, T. W., and Park, E. D. (2016). "CO and CO_2 methanation over supported Ni catalysts," *J. Catalysis Today* 293-294, 89-96. DOI: 10.1016/j.cattod.2016.12.036

Li, K. X., Yang, X. H., Zhao, T. T., Liu, J. J., Liu, J. H., Li, Y. C., Li, F. H., Tai, X. S., and Cao, S. H. (2019). "Raney Ni as recyclable and selective catalyst for the reduction of α-pinene to cis-pinane with $NaBH_4$ at room temperature," *J. ChemistrySelect* 4(35), 10506-10509. DOI: 10.1002/slct.201902769

Li, M. S., Wang, X. D., Li, S. R., Wang, S. P., and Ma, X. B. (2010). "Hydrogen production from ethanol steam reforming over nickel based catalyst derived from Ni/Mg/Al hydrotalcite-like compounds," *J. International Journal of Hydrogen Energy* 35(13), 6699-6708. DOI: 10.1016/j.ijhydene.2010.04.105

Li, X. Z., Qin, F., Dai, Q. G., Shao, S. J., and Wang X. Y. (2018). "Hydrogenation–dechlorination of 2-chloro-4, 6-dinitroresorcinol over Pd/C catalysts," *J. Research on Chemical Intermediates* 44(10), 6087-6104. DOI: 10.1007/s11164-018-3477-y

Moutombi, F. J. N., Selka, A., Fabiano-Tixier, A. S., Foucher, D., Clarisse, O., Chemat, F., and Touaibia, M. (2018). "Highly selective solvent-free hydrogenation of pinenes to added-value cis-pinane," *J. Comptes Rendus Chimie* 21(11), 1035-1042. DOI: 10.1016/j.crci.2018.09.002

Narayan, S., Muldoon, J., Finn, M., Fokin, V. V., Kolb, H. C., and Sharpless, K. B. (2005). " 'On water': Unique reactivity of organic compounds in aqueous suspension," *J. Angewandte Chemie International Edition* 44(21), 3275-3279. DOI: 10.1002/ange.200462883

Nuttens, N., Verboekend, D., Deneyer, A., Van Aelst, J., and Sels, B. F. (2015). "Potential of sustainable hierarchical zeolites in the valorization of alpha-pinene," *J. ChemSusChem* 8(7), 1197-1205. DOI: 10.1002/cssc.201403457

Ryzhikov, A., Ronchi, L., Nouali, H., Daou, T. J., Paillaud, J. L., and Patarin, J. (2015). "High-pressure intrusion–extrusion of water and electrolyte solutions in pure-silica LTA zeolite," *J. Physical Chemistry C* 119(51), 28319-28325. DOI: 10.1021/acs.jpcc.5b09861

Selka, A., Levesque, N. A., Foucher, D., Clarisse, O., Chemat, F., and Touaibia, M. (2017). "A comparative study of solvent-free and highly efficient pinene hydrogenation over Pd on carbon, alumina, and silica supports," *J. Organic Process Research & Development* 21(1), 60-64. DOI: 10.1021/acs.oprd.6b00344

Shao, M. Q., Cui, H. T., Guo, S. Q., Zhao, L. F., and Tan, Y. S. (2018). "Effects of calcination and reduction temperature on the properties of Ni-P/SiO_2 and Ni-P/Al_2O_3 and their hydrodenitrogenation performance," *RSC Advances* 8(13), 6745-6751. DOI: 10.1039/c7ra11907k

Shi, Y. M., Guo, Z. J., Wang, Q., Zhang, L. Y., Li, J., Zhou, Y., and Wang, J. (2017). "Amphiphilic mesoporous poly (ionic liquid) immobilized heteropolyanions towards the efficient heterogeneous epoxidation of alkenes with stoichiometric hydrogen peroxide," *ChemCatChem* 9(23), 4426-4436. DOI: 10.1002/cctc.201700906

Slater, C. S., Savelski, M. J., Carole, W. A., and Constable, D. J. (2010). "Solvent use and waste issues," *Green Chemistry in the Pharmaceutical Industry* 49-82. DOI: 10.1002/9783527629688

Tanielyan, S., Biunno, N., Bhagat, R., and Augustine, R. (2014). "Anchored Wilkinson catalyst: hydrogenation of β pinene," *J. Topics in Catalysis* 57(17), 1564-1569. DOI: 10.1007/s11244-014-0332-2

Wang, F., Feng, T., Jin, X. J., Zhou, Y. L., Xu, Y. J., Gao, Y. H., Li, H. S., and Lei J. F.

(2021). "Atomic Co/Ni active sites assisted MOF-derived rich nitrogen-doped carbon hollow nanocages for enhanced lithium storage," *Chemical Engineering Journal* 420, article 127583. DOI: 10.1016/j.cej.2020.127583

Wang, J. G., Liu, H. Z., Sun, H. H., Hua, W., Wang, H. W., Liu, X. R., and Wei, B. Q. (2018). "One-pot synthesis of nitrogen-doped ordered mesoporous carbon spheres for high-rate and long-cycle life supercapacitors," *J. Carbon*, 127, 85-92. DOI: 10.1016/j.carbon.2017.10.084

Wang, L. L., Guo, H. Q., Chen, X. P., Huang, Y. Y., and Zhang, P. P. (2015). "Hydrogenation of pinene on spent fluid cracking catalyst supported nickel: Langmuir–Hinshelwood kinetic modelling," *J. Reaction Kinetics, Mechanisms and Catalysis* 114(2), 639-660. DOI: 10.1007/s11144-014-0816-x

Wei, X. R., Zhou, M. Y., Zhang, X. C., Wang, X. N., and Wu, Z. X. (2019). "Amphiphilic mesoporous sandwich-structured catalysts for selective hydrogenation of 4-nitrostyrene in water," *ACS Applied Materials & Interfaces* 11(42), 39116-39124. DOI: 10.1021/acsami.9b14141

Xie, R. L., Zhang, X., Tian, Y. J., Lei, Z., and Cao, E. D. (2021). "Nitrogen-doped porous carbon supported nickel nanoparticles as catalyst for catalytic hydroconversion of high-temperature coal tar," *Journal of Fuel Chemistry and Technology* 49(10), 1402-1411. DOI: 10.1016/s1872-5813(21)60156-1

Xiong, R. J., Zhao, W. Q., Wang, Z. Q., and Zhang, M. H. (2020). "A sulfur-tolerant phosphorus doped Pd/C catalyst for hydrogenation of 4-nitrothioanisole," *J. Molecular Catalysis* 5000, article 111332. DOI: 10.1016/j.mcat.2020.111332

Xu, M. C., Zhou, Y., and Huang, J. H. (2008). "Adsorption behaviors of three polymeric adsorbents with amide groups for phenol in aqueous solution," *Journal of Colloid and Interface Science* 327(1), 9-14. DOI: 10.1016/j.jcis.2008.07.054

Yang, C., Jiang, L. H., Wang, H. B., Zheng, Y. E., and Wang, Y. M. (2018). "Process optimization for selective hydrogenation of α-pinene over Ni/$AlPO_4$," *J. Korean Journal of Chemical Engineering* 35(2), 409-420. DOI: 10.1007/s11814-017-0307-7

Yang, Y. G., Liu, X. X., Yin, D. L., Zhang, Z. H., Lei, D. C., and Yang, J. (2015). "A recyclable Pd colloidal catalyst for liquid phase hydrogenation of α-pinene," *Journal of Industrial and Engineering Chemistry* 26, 333-334. DOI: 10.1016/j.jiec.2014.12.005

Yin, L., Tian, Q., Boyjoo, Y., Hou, G. J., Shi, X., and Liu J. (2019). "Synthesis of colloidal mesoporous silica spheres with large through-holes on the shell," *Langmuir* 36(25), 6984-6993. DOI: 10.1021/acs.langmuir.9b03179

Zhou, F., Hearne, Z., and Li, C. J. (2019). "Water—the greenest solvent overall," *Current Opinion in Green and Sustainable Chemistry* 18, 118-123. DOI: 10.1016/j.cogsc.2019.05.004

Zhou, J. S., Lian, J., Hou, L., Zhang, J. C., Gou, H. Y., Xia, M. R., Zhao, Y. F., Strobel, T. A, Tao, L., and Gao, F. (2015). "Ultrahigh volumetric capacitance and cyclic stability of fluorine and nitrogen co-doped carbon microspheres," *Nature Communications* 6(1), 1-8. DOI: 10.1038/ncomms9503

Article submitted: April 3, 2023; Peer review completed: April 15, 2023; Revised version received and accepted: April 19, 2023; Published: April 24, 2023.
DOI: 10.15376/biores.18.2.4032-4054

APPENDIX

Supplementary Material

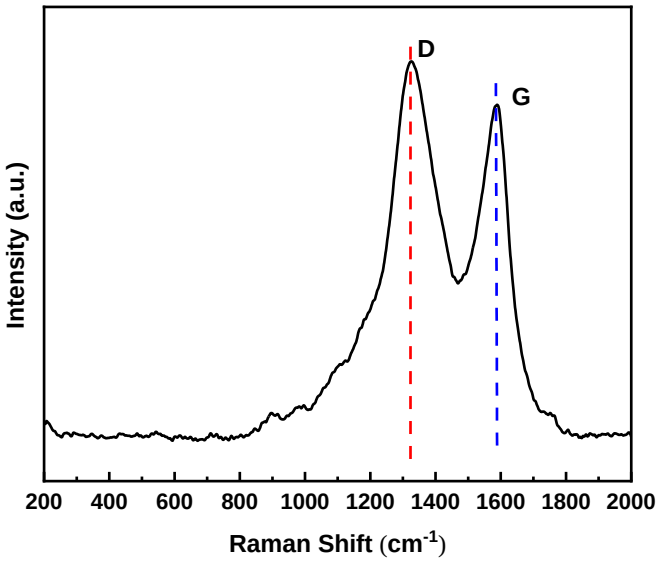

Fig. S1. Raman spectrum of N-C@MS

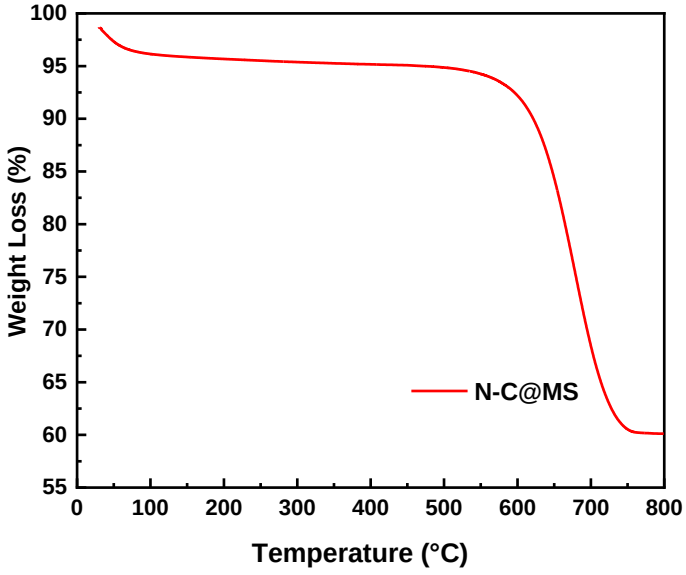

Fig. S2. TG curve of N-C@MS

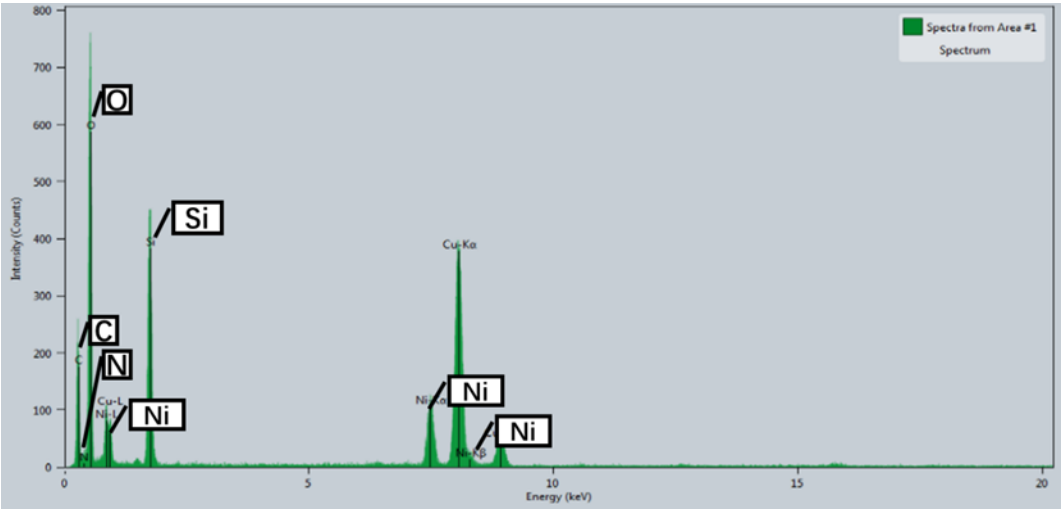

Fig. S3. EDX full scan of Ni/N-C@MS

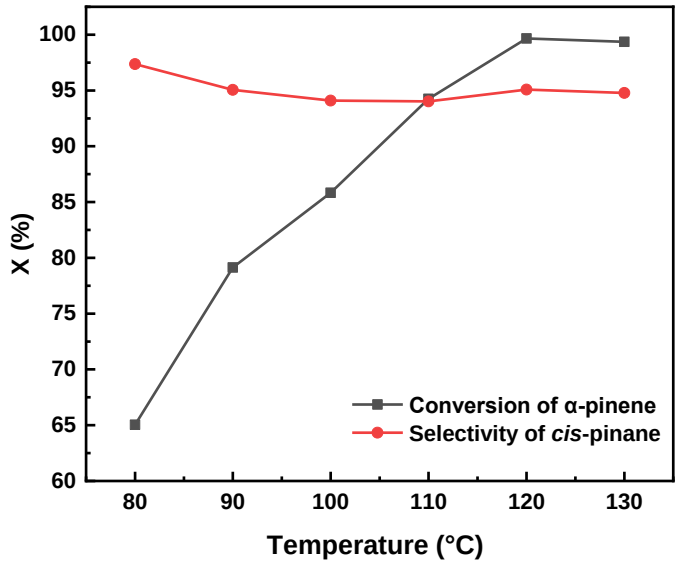

Fig. S4. Effect of temperature on hydrogenation of α-pinene

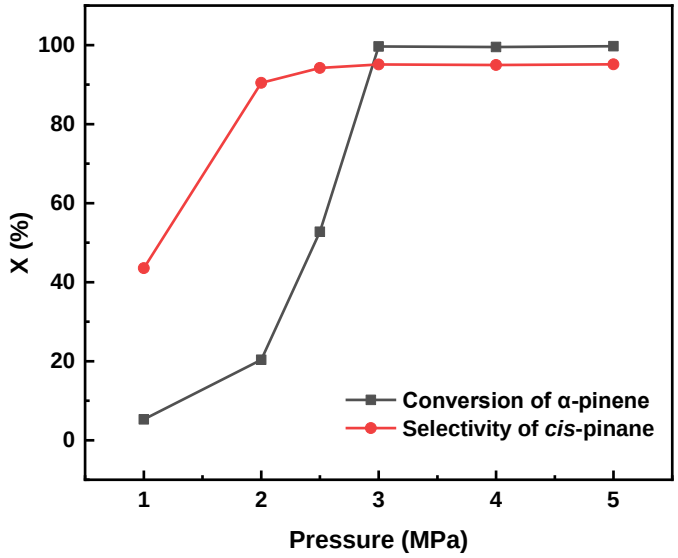

Fig. S5. Effect of hydrogen pressure on hydrogenation of α-pinene

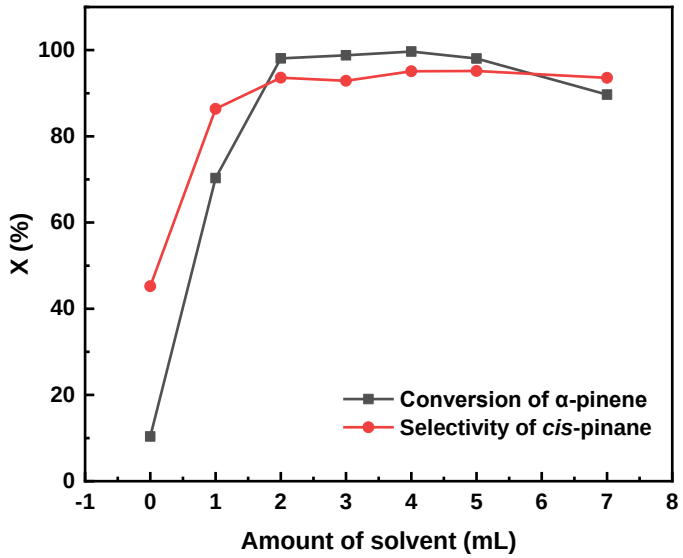

Fig. S6. Effect of solvent amount on hydrogenation reaction of α-pinene

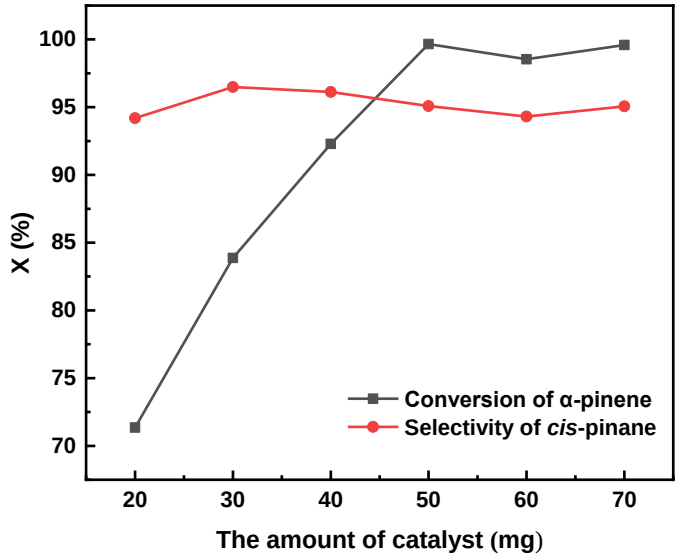

Fig. S7. Effect of catalyst dosage on hydrogenation of α-pinene

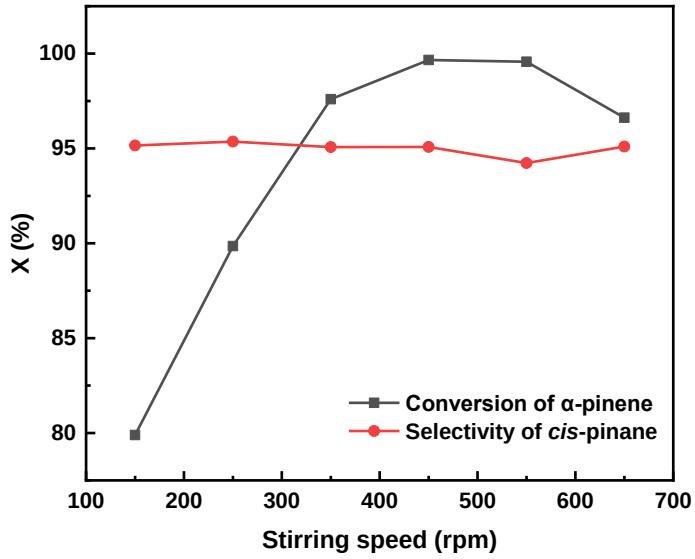

Fig. S8. Effect of stirring speed on hydrogenation reaction of α-pinene

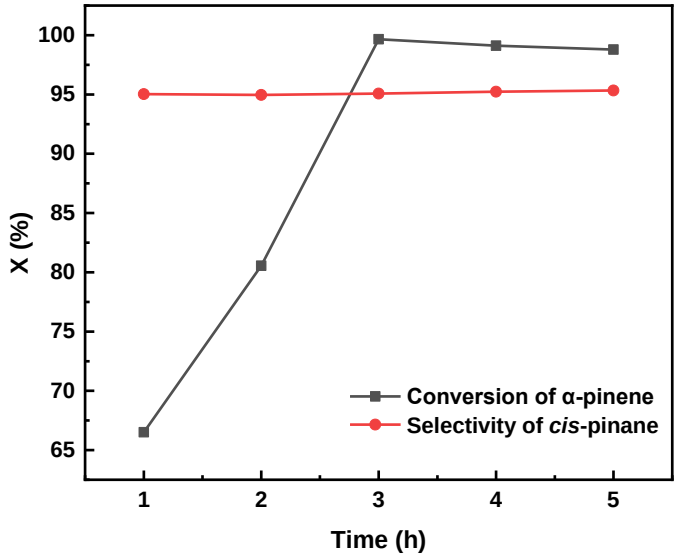

Fig. S9. Effect of reaction time on hydrogenation of α-pinene